J Comp Physiol A (2005) 191: 761–775
DOI 10.1007/s00359-005-0631-y

ORIGINAL PAPER

Jacob L. Krans · William D. Chapple

Variability of motoneuron activation and the modulation of force production in a postural reflex of the hermit crab abdomen

Received: 20 October 2004 / Revised: 15 March 2005 / Accepted: 16 March 2005 / Published online: 1 July 2005

Abstract The tri-phasic reflex in hermit crab (*Pagurus pollicarus*) abdomen is triggered by local mechanoreceptors and is essential for postural control. The reflex consists of three stereotypical phases: a brief, high-frequency burst, a transient cessation of firing, and a late-discharge that is much lower in frequency than the initial burst. To better understand the reflex generation of force, variability of motoneuron discharge in each of five parameters of reflex activation was assessed. An intracellular current injection routine was used to correlate each of these parameters with force production. Phase 3 motoneuron firing frequency showed the greatest correlation with force production. Phase 3 spike rate increased as a function of phase 2 duration, but the relationship between phase 2 duration and force produced by the reflex was weak. Junction potential amplitude decreased as phase 2 duration increased, and we hypothesize that this trend counteracts the increased phase 3 frequency, explaining the weak relationship of phase 2 duration and force production. Surprisingly, when phase 3 frequency was held constant and phase 2 was increased in duration, the concurrent decrease in junction potential amplitude did not reduce force production.

Keywords Crustacean · Postural control · Reflex · Motoneuron · Force

Abbreviation VSM: Ventral superficial muscle · VSMN: Ventral superficial muscle motoneurons · pps: Pulses per second · SFA: Spike frequency adaptation · PSDF: Probability spike density function

J. L. Krans (✉) · W. D. Chapple
Department of Physiology and Neurobiology,
University of Connecticut, Storrs, CT 06269, USA
E-mail: jlk68@cornell.edu
Tel.: +1-607-2544317

Present address: J. L. Krans
Department of Neurobiology and Behavior,
Cornell University, W214 Mudd Hall, Ithaca, NY 14853, USA

Introduction

We are interested in the neural mechanisms by which the hermit crab, *Pagurus pollicarus*, controls its shell position during normal behavior (Chapple 1973a, b). The abdomen of *Pagurus* is de-calcified and wraps around the inner columella of large gastropod shells. Shells serve as protection from ocean predators and are carried, rather than dragged, during normal behavior (Kitabayashi et al. 2002; Turra and Denadai 2002). The tonic motor system of the abdomen has evolved to manage this relatively specialized task of lifting a shell that exerts many times the downward force of the animal itself. Recent work has focused on a description of the tri-phasic reflex activation of motoneurons that are important for this postural control (Chapple and Krans 2004). The reflex consists of three characteristic phases of spiking from postural motoneurons and is triggered by mechanoreceptors of the abdomen. The first of these phases (phase 1) is a high-frequency burst of action potentials that lasts about 100 ms. Spike frequency during phase 1 decays in rate and transitions into phase 2. Phase 2 is a cessation of firing that is generated by premotor inhibitory synaptic events local to each abdominal ganglion and intrinsic spike frequency adaptation of the motoneurons (Chapple and Krans 2004; Krans and Chapple 2005). The third and final phase is defined by a firing rate that is greater than tonic spike frequency, but much less than that of the initial burst. Investigations of the intact animal and of reduced abdominal preparations have shown that the force generated by the reflex can widely vary (Krans and Chapple 2005). This variation in force production has not yet been correlated to the sensory spike rate that triggers it, to any of the parameters of motoneuron spiking during the reflex, nor to changes at the neuromuscular junction.

The functional contribution of the second reflex phase of motoneuron discharge, a transient cessation of firing, has been particularly elusive in our characterization of this reflex. In a recent report, we showed that this pause in motoneuron firing attenuates intrinsic spike frequency adaptation and may permit greater spike rates in the late-discharge of the reflex: phase 3 (Krans and Chapple 2005). We hypothesized that this action on motoneuron rate would modulate reflex force generation, perhaps accounting for an important source of variability and illustrating a functional implication of the intrinsic spike frequency adaptation of the postural motoneurons.

A model preparation in which numerous variables are well described and accessible for experimental manipulation does not currently exist for the study of neural networks involved in the tonic maintenance of posture. Moreover, the behavioral consequence of specific modulation to individual components of these networks continues to be difficult to quantify. It is useful to examine preparations in which several, if not all, components may be observed or experimentally controlled; there are methodological restrictions in many mammalian preparations that make studies of this type more difficult (Magarinos-Ascone et al. 1999). This deficit has been addressed by several investigators, but remains a relatively poorly populated area of research (Beloozerova et al. 2003; Fung and Macpherson 1999; Harris-Warrick and Kravitz 1984; Horak and MacPherson 1996; Ma et al. 1992; Noah et al. 2004; Ridgel et al. 2000; Zill 1987). The postural system of the abdomen of *Pagurus* offers several advantages for investigating tonic maintenance of posture. Normal *Pagurus* behavior requires that the postural system compensate for constantly changing torques of considerable magnitude, as well as the static and dynamic loads exerted along the abdomen-shell contact area. This is accomplished by the superficial muscle layers of the abdomen in conjunction with the fourth and fifth walking appendages of the thorax (Chapple 1973a, b). Intracellular recording from these muscles, as well as extracellular recording from afferent and motor nerves is easily attainable. Intracellular recording from superficial muscle motoneurons is more difficult, but is reproducibly feasible.

We have investigated the variability present in the duration and spike frequency of each of the three reflex phases in an effort to identify portions of the reflex involved in modulating force production. Previous investigations illustrated that a single afferent potential is sufficient to trigger the reflex (Krans and Chapple 2005), that spontaneous afferent potentials that occur during reflex activation of the motoneurons do not reset the reflex (Chapple and Krans 2004), and that the excitatory synaptic potentials that depolarize postural motoneurons during the initial reflex phase have relatively little variability (Krans and Chapple 2005). These observations suggest that neither the variability of afferent spiking, nor the synaptic depolarization of phase 1 are primary sources of modulation in the reflex production of force. In experiments reported here, a three-phase intracellular depolarization protocol and an axonal stimulation protocol were used to examine the action of individual parameters of tri-phasic motoneuron firing on force production.

Methods

Collection and dissection of *P. pollicarus* were modified only slightly from a recent report, in which a schematic of the preparation and recording sites is provided (Krans and Chapple 2005). Modifications to those methods as well as critical methods are described below.

The right first nerve was preferentially used for afferent stimulation experiments; it is composed almost entirely of sensory afferents. Two preparations were used: (1) the semi-intact abdominal nervous system, consisting of all five abdominal ganglia and typically just one muscle segment. In this preparation, all nerves were cut peripheral to the connectives except for one motor nerve (the third nerve) that was left innervating muscle for force recordings. The afferent nerve was cut distally and drawn into a suction electrode for electrical stimulation. In experiments where force measurements were not necessary, the motor nerve was cut distally and potentials were recorded with a suction electrode. (2) The isolated ganglion preparation; the fourth ganglion was physically isolated from the abdominal nerve cord by severing the 3–4 and 4–5 connectives close to the third and fifth ganglia. The recording and stimulation procedures were the same in both preparations.

Spiking in the lateral superficial motoneurons was avoided in some experiments because of its grossly nonlinear force generation; lateral muscle fibers can produce spikes. The right motor nerve of the ganglion was used during electrical stimulation of motoneuron axons because the threshold for the lateral, in this ganglionic nerve, is greater than the other motoneurons and may thus be excluded. On the left side, the medial ventral superficial muscle motoneuron (VSMN) shows the largest extracellular potential, corresponding to the largest axon diameter. Electrical stimulus intensity was adjusted such that the medial, but not the lateral VSMN was recruited. This was confirmed using two methods, both of which are shown (e.g., Fig. 7a): (1) inspection of an extracellular recording of the motor nerve, recorded peripheral to the stimulus site, and (2) inspection of excitatory junction potentials (ejps) in all longitudinal muscle groups (medial muscle is shown; no ejps occurred in other muscles).

Solutions and data acquisition

Preparations were maintained at 12.5°C in Cole's solution during experiments (in mM/l): NaCl 460, KCl 15.7, $CaCl_2$ 25.9, $MgCl_2{\cdot}6H_2O$ 8.3, Na_2SO_4 8.4, buffered with HEPES to pH 7.4. A high Ca^{++}, Mg^{++} saline (HCM) was used in some experiments: NaCl 408.7, KCl 15.7,

$CaCl_2$ 64.75, $MgCl_2 \cdot 6H_2O$ 20.75, Na_2SO_4 8.4. HCM was both applied to the nerve cord within the confines of a Vaseline well atop a Sylgard (Dow Corning Corporation, NY, USA) pedestal within the recording chamber. This arrangement minimized physical strain to the motor nerve as it exited the Vaseline barrier without changing elevation to innervate the muscle; muscle segments were slightly elevated by the arrangement of plastic tabs used for force measurements.

Extracellular potentials from the motor nerve were recorded either with polyethylene or glass suction electrodes. A hook electrode was used in some experiments to record potentials in the afferent root during and after electrical stimulation. Signals were amplified with a differential AC amplifier with a passband of 10 Hz – 1 kHz and digitized at 5 kHz with user-composed routines and a CED Power 1401 Data acquisition system (A-M Systems, Inc., Carlsburg, WA, USA; Spike5 and Signal v.2 software, Cambridge Electronic Design (CED), Cambridge, England). Intracellular recordings were made from desheathed ganglia using 40–80 MΩ glass micropipettes, filled with 2 M potassium acetate, using an AxoClamp 2B amplifier (Axon Instruments, Union City, CA, USA). All intracellular recordings were made in either bridge or DCC mode of the AxoClamp. Multistep current injection protocols were executed using DAC outputs on the CED 1401 and the AxoClamp 2B. Forces were recorded using a force transducer attached to plates that were glued to the cuticle of the third and fifth right segments. The ventral superficial muscle (VSM) and corresponding motor nerve were used for experiments involving force measurements. Muscle segments contralateral to the motor nerve being observed were removed to eliminate confounding force production. This permitted the correlation of force production and motor nerve activity. A pseudorandom number table was generated using Matlab (The MathWorks, Inc., Natick, MA, USA) and used to vary the order of current magnitudes injected to motoneuron. There were between 10 and 30 repetitions of each experimental manipulation. For these repetitions the intertrial pause was varied randomly about a mean value of about 57s. For a given motoneuron, during experiments of depolarizing current injection, the number of spikes per trial (whole tri-phasic discharge) was typically greater than 20. After 10 or more repetitions, this provided spike counts well into the hundreds for any given experimental condition and generally these counts were in the thousands.

Criteria for intracellular identification of the ventral superficial muscle motoneurons have been described in detail (Chapple and Krans 2004; Krans and Chapple 2005).

Data analysis

Records of extracellular spike rate, intracellular membrane potential (motoneurons and muscle fibers), and force were displayed and analyzed using custom composed routines in Matlab (The MathWorks, Inc, Natick, MA, USA). Extracellular amplitude computation has been described in detail (Krans and Chapple 2005). An amplitude histogram of all the spike amplitudes observed from the motor nerve was constructed. The upper and lower boundaries of a chosen histogram peak were then selected to define a single motor unit.

As described in previous reports (Chapple and Krans 2004), we have chosen to use the probability spike density function (PSDF) as a means of providing a continuous approximation of spike rate probability computed from numerous repetitions of a particular experimental design. Peristimulus time histograms and rasters may be graphically preferable to the PSDF, but do not permit simple computation of continuous variance/deviation. The width of the Gaussian kernel (standard deviation) is typically five times that of the sampling window and thus yields nonzero probabilities preceding individual spikes, which may obscure graphical interpretation (Fig. 1b, bottom). In the present experiments the function is used to provide a continuous approximation so that variance may be computed.

Linear, exponential, logarithmic, and parabolic equations used to fit data were generated using *basic fitting*, *polyfit*, and *exp* routines in Matlab. These equations are given in figure legends rather than text and are reported as general equations.

Results

An example of the initial second of afferent triggered reflex activation of motoneurons and the resultant junction potentials and force are shown in Fig. 1; reflex discharge is typically several seconds. Reflex motoneuron discharge can be recorded from all motoneurons simultaneously by recording *en passant* from the third nerve of each abdominal ganglion (Fig.1a), or individually via sharp electrode penetration within the ganglia (Krans and Chapple 2005). The largest amplitude extracellular potential in the example of Fig. 1a is from the medial VSMN and exhibits the prototypical reflex firing sequence [only a portion of which is shown in Fig. 1a, (see Chapple and Krans 2004) for more examples]. The resultant change in membrane potential of the medial muscle is shown just below the extracellular recording of VSMN activity. In this example, phase 1 consisted of three spikes from the medial motoneuron that generated a compound ejp. The muscle depolarization generated by the initial phase 3 spike (filled arrowhead) was only slightly less than that of the compound potential of phase 1. This illustrates neuromuscular facilitation that is common at the neuromuscular junction of *Pagurus* and in general of crustacean tonic neuromuscular junctions (Atwood 1967; Millar et al. 2002; Zucker and Regehr 2002). The force produced by the reflex consists of a marked inflection at the onset of the third phase, which is shown in the final panel of Fig. 1a.

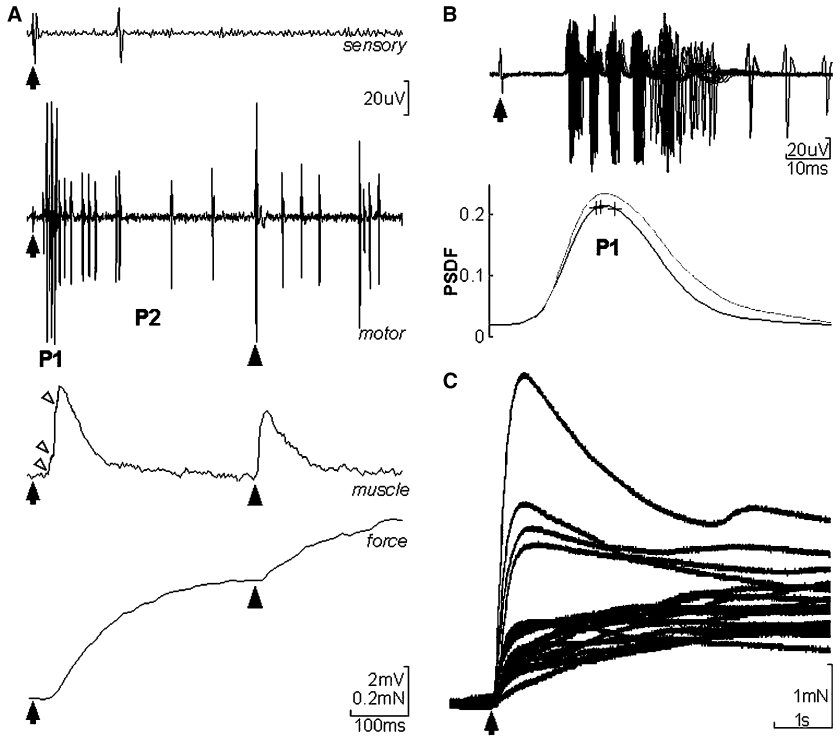

Fig. 1 Afferent triggered reflex activation of motoneurons and resultant peripheral action **a** From *top* to *bottom*: extracellular recording from the afferent nerve (first) of the fourth abdominal ganglion following electrical stimulus (*filled arrow*, throughout) peripheral to the recording site. Simultaneously recorded extracellular trace from the motor nerve of the fourth abdominal ganglion is shown below. Four classes of extracellular potentials are present. The largest of these is the medial VSMN. About one second of motor activity is depicted. This period shows the brief burst of phase 1 (*P1*), a relatively long duration phase 2 (*P2*), and the beginning of phase 3 (*filled arrowhead*). The resultant depolarization in the medial muscle is shown beneath the motor nerve trace. Note that the first depolarization consists of three neuromuscular events (*open arrowheads*), and that the only phase 3 medial action potential shown in panel B generates an ejp of comparable amplitude to the initial compound potential (*filled arrowhead*). Longitudinal force produced by the tri-phasic activation in the previous three panels is shown in the *bottom panel* of **a**. Note the inflection in the rise of force upon a single phase 3 motoneuron spike. The force generated by that single spike (*filled arrowhead*) is only slightly less than that produced by all three phase 1 potentials. **b** *Top* ten individual records, superimposed, after single electrical stimuli were delivered to the afferent nerve (*filled arrow*). *Bottom* probability spike density function (*PSDF*) computed from 30 trials of the motor spike trains *shown above*. Three points about the peak are selected for further analysis (+). Probability of firing at these points is 0.190 ± 0.020, 0.192 ± 0.021, and 0.189 ± 0.021 (*left* to *right*), and coefficients of variance are 0.105, 0.107, 0.111 (*left* to *right*). *Gray* a continuous plot of deviation (PSDF + 1SD). **c** longitudinal force produced by VSMN over 15 repetitions of equivalent electrical stimuli to the afferent nerve (*filled arrow*). These traces were recorded in a single series of stimulus repetitions to the same preparation

Variance intrinsic to each phase of reflex motoneuron firing

Though phase 1 motoneuron spike rate changes little across trials with varied afferent spiking, there is notable variability in force production (Fig. 1b, c). A typical example of phase 1 motoneuron spiking is depicted in Fig. 1b. Ten traces of the initial motoneuron discharge, which is triggered by equivalent single stimuli to the afferent nerve, are superimposed onto one another in Fig. 1b. The number of spikes that occur is fairly consistent within a single preparation and at a given stimulus intensity (Fig. 1b, Table 1). The PSDF computed from all 30 trials of this experiment appears beneath the overlaid extracellular potentials. Mean coefficient of variance was computed from the PSDF near the phase 1 peak probability of motoneuron firing for comparison with variance in force produced by the reflex. The mean CoV during the time encapsulated by points shown in Fig. 1b (crosses) was 0.108 ($\pm$ 0.002). The force generated by reflex activation, in trials depicted in Fig. 1b, is plotted in Fig. 1c on a longer time scale. The CoV of peak force is about eight fold greater than that of phase 1 frequency (peak force: mean $\pm$ SD = 1.48 ± 1.31 mN, CoV = 0.88). This suggests that phase 1 frequency is not a likely source of modulation of the final reflex force.

We quantified the variability present in each of the five parameters of the tri-phasic activation of VSMN in an effort to identify those parameters with the greatest operational range as putative contributors to the variability in force production: (1) phase 1 frequency, (2) phase 1 duration, (3) phase 2 duration, (4) phase 3 frequency and (5) phase 2 duration. Phase 2 frequency was not assessed; phase 2 is a cessation or gross reduction in spiking. Each parameter was measured from data recorded from ten semi-intact abdominal preparations of at least 20 repetitions each, after a single electrical stimulus to the afferent nerve. The efficacy of single

Table 1 Five parameters of tri-phasic reflex activation of motoneurons, computed from seven preparations(n = trials per preparation)

Experiment	n	Phase 1 duration (ms)			Phase 1 frequency (Hz)			Phase 1 number of spikes			Phase 2 duration (ms)			Phase 3 duration (ms)			Phase 3 frequency (Hz)		
		Mean	±SD	CoV	Mean	±SD	CoV	Mean	±SD	CoV	Mean	±SD	CoV	Mean	±SD	CoV	Mean	±SD	CoV
1	30	100.6	11.9	0.12	126.3	38.83	0.31	2.67	1.47	0.55	597.6	304.6	0.51	2.85	1.69	0.59	6.083	2.66	0.44
2	20	43.1	5.9	0.14	198.6	94.31	0.47	4.65	1.84	0.4	211.8	98.6	0.47	2.46	1.48	0.6	13.60	6.97	0.51
3	20	111.2	61.5	0.55	131.2	25.23	0.19	5.1	0.85	0.17	334.2	168.0	0.5	5.36	2.12	0.4	5.36	2.12	0.4
4	30	172.6	20.8	0.12	139.2	56.28	0.4	10.23	2.53	0.25	898.5	619.1	0.69	1.41	0.59	0.42	3.98	2.16	0.54
5	30	159.4	56.8	0.36	92.42	12.03	0.13	8.5	2.30	0.27	572.4	268.4	0.47	3.66	0.76	0.21	17.00	4.51	0.27
6	10	61.4	11.9	0.19	45.65	23.27	0.51	3.7	1.25	0.34	1270.1	665.3	0.52	2.75	2.79	1.01	22.75	8.57	0.38
7	20	135.7	53.1	0.39	98.36	21.18	0.22	4.25	0.91	0.21	661.0	257.9	0.39	3.021	0.67	0.22	14.87	8.25	0.55

afferent potentials, recruited by electrical stimulation of the afferent nerve, in triggering the reflex has been shown to be comparable to reflexes driven by mechanical perturbation (Chapple and Krans 2004). The seven preparations that most closely resembled data gathered in experiments of mechanical stimulus to semi-intact abdominal preparations were chosen for analysis and are shown in Table 1 and Fig. 2 (Chapple and Krans 2004). Table 1 lists the mean, standard deviation, and CoV values of each reflex parameter in original units; before normalization and concatenation for further analysis. These data were normalized to the mean value within each preparation, and each parameter or reflex activation, so that variance could be analyzed across preparations (histograms, Fig. 2).

We determined simple indications of the start and stop times for a given phase because the phases of VSMN reflex activation are not discrete; each gradually progresses to the next. Tonic firing frequency was used as a threshold value such that a deviation greater than one standard deviation indicated the start or stop of a phase (Fig. 2a, mean tonic frequency: dotted line, SD solid line). For example, phase 3 start time is the upward deviation from the envelope defined by the mean tonic firing rate (computed in trials interspersed between stimulus trials) plus one standard deviation, and its end was the downward return. Figure 2a shows instantaneous frequency data computed from reflex activation of VSMN in one preparation, over 20 trials, that is generally representative of the tri-phasic motoneuron discharge (mean tonic rate: dotted, one SD solid). The method of determining start and stop times that is described above provided a consistent metric across all preparations and motoneurons investigated.

Figures 2b–f are histograms of these data, and illustrate the general distribution and variance of each reflex parameter investigated. The CoV values of phase 1 duration and frequency were 0.27 and 0.32, respectively, and were the smallest observed values (Fig. 2b, c). Although phase 1 frequency decays rapidly and substantially, generating a wide range of instantaneous frequencies in a short period (Krans and Chapple 2005), the CoV was still less than those computed for phase 2 and 3 distributions. The parameter with the greatest CoV was the duration of phase 2 (Fig. 2d; CoV = 0.51). The CoV of phase 3 frequency was 0.44, and duration: 0.49 (Fig. 2e, f). These measures of variance in afferent triggered reflexes indicate that the reflex parameters with the widest ranges, throughout which modulation of force production may occur, are phases 2 and 3. We thus directed our investigation toward the actions of phase 2 and phase 3 on final force production.

Reflex parameters, an intracellular current injection protocol

A protocol to generate tri-phasic activation of VSMN, via intracellular current injection, was designed for this

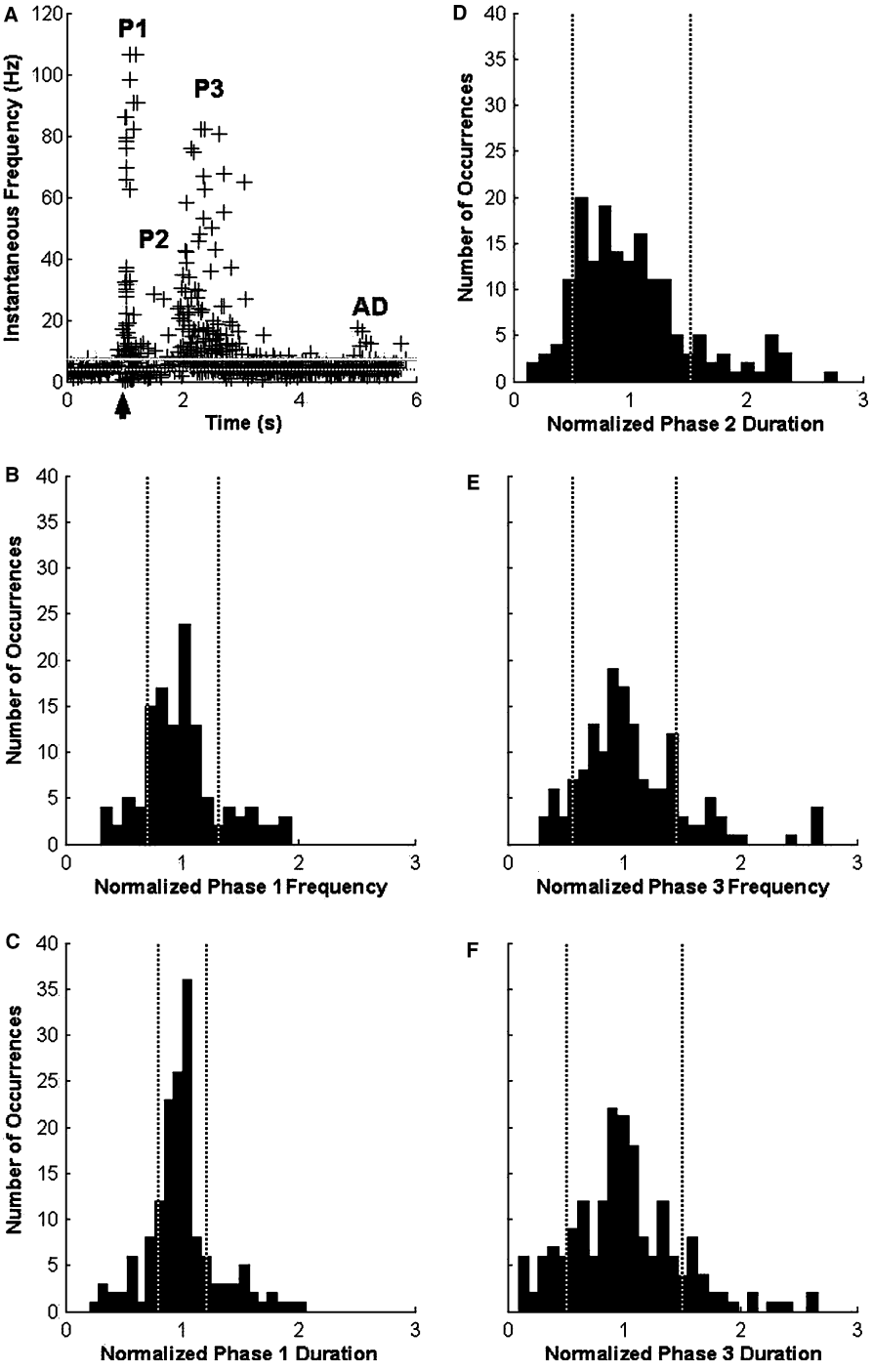

Fig. 2 Variability within the tri-phasic reflex **a** instantaneous frequency of the medial VSMN over 20 trials of single stimulus to the afferent root (*filled arrow*, $t = 1$). P1, P2, and P3 indicate the first, second, and third phases, respectively. In two trials of these 20, a later, after-discharge (*AD*) of VSMN spiking occurred (see text). The initial portion of this after-discharge occurs in the time period that is plotted in **a**. *Dotted line*: the mean spike rate, computed in the absence of afferent stimulus. *Solid line:* one standard deviation above mean spike rate. **b** histogram of phase 1 frequency normalized to the mean value per preparation ($n = 7$ preparations, all panels; $n = 160$ stimulus trials). CoV of distributions is plotted as dotted vertical lines in **b–f**. Likewise, **C–F** are histograms of normalized phase 1 duration ($n = 140$ trials), phase 2 duration ($n = 160$ trials), phase 3 frequency ($n = 150$ trials), and phase 3 duration ($n = 180$ trials), respectively. Nonnormalized data from these experiments are given in Table 1

investigation. This design permitted examination of the relationships between each parameter of the tri-phasic discharge and final force production, independently. A three-step intracellular current injection paradigm was used to drive motoneuron spike rates comparable to those observed in the afferent triggered reflex (Fig. 3a). We modeled the tri-phasic spike pattern by passing a brief depolarizing current, then transiently repolarizing the membrane to rest, and finally passing a longer pulse of depolarizing current that was lesser in magnitude than the first (Fig. 3a, bottom). The range through which we varied each of the five parameters of tri-phasic firing was determined by previous computations of CoV, which were made from more behaviorally relevant values; afferent triggered reflexes in the semi-intact abdominal preparation. With the exception of phase 3 duration, the experimental range of each parameter was designed to account for the majority of values reported in Table 1. In previous reports we have commented on the sporadic presence of a very long lasting phase 3 discharge. This

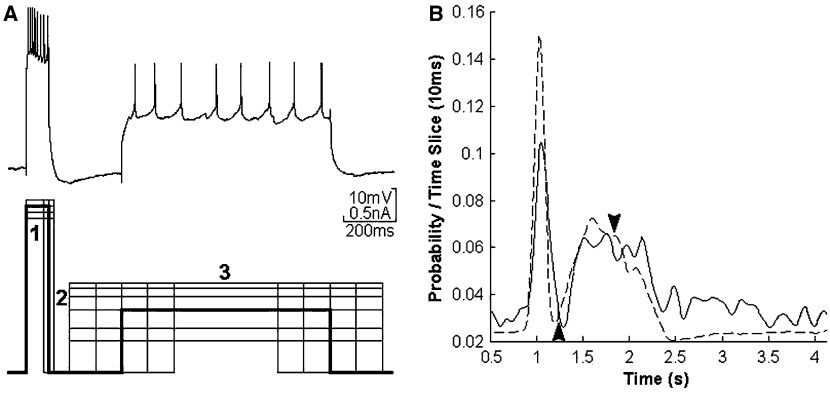

Fig. 3 Artificial tri-phasic experimental design **a** *Top* Intracellular voltage recording from the medial VSMN during a trial of the artificial tri-phasic waveform experiments. *Bottom* injected current paradigm for this series of experiments. Changes in duration and magnitude of each phase are depicted by *thin lines*. The voltage recording in the *top panel* was generated by current injection depicted by the *thick line* in the *bottom panel*. 1, 2 and 3 indicate the approximated first, second, and third phases. **b** Comparison of probability spike density function approximations of spike frequency from afferent triggered tri-phasic reflex discharge (*solid line*) and spiking generated by intracellular current injection (*dashed line*). *Arrowheads* indicate the times at which mean and SD of the PSDF (reported in Results) are computed

late discharge from the postural motoneurons can last several seconds, is generated by variable rate and amplitude excitatory synaptic potentials, and shows erratic variation in spike rate from trial to trial (Chapple and Krans 2004); it does not occur with every presentation of equivalent stimuli. In contrast to phase 3, this discharge generally occurs after a brief return to tonic spike rate in VSMN and is always substantially longer than the preceding phase 3 duration (e.g., AD in Fig. 2a). Based on these observations and to simplify our analysis in these experiments, the duration of phase 3 was varied over only a short proportion of the range observed in afferent triggered reflex discharges (range = 600–1000 ms, as shown in Fig. 3a).

The PSDF was used to confirm that the artificial tri-phasic protocol described above approximated afferent triggered reflex discharge (Fig. 3b; dashed: depolarization generated tri-phasic discharge, solid: afferent triggered reflex discharge). PSDF mean and standard deviation was computed at time points throughout phase 2 and phase 3 to compare afferent triggered and intracellular driven tri-phasic spiking. In the example shown, these probabilities were: afferent phase $2 = 0.26 \pm 0.031$, intracellular phase $2 = 0.28 \pm 0.021$; and afferent phase $3 = 0.66 \pm 0.079$, intracellular phase $3 = 0.73 \pm 0.044$ (mean PSDF $\pm$ SD; afferent trials ($n = 30$) versus intracellular trials ($n = 20$) $P > 0.05$, each phase). Phase 1 probability of firing observed in intracellular driven tri-phasic discharge was always greater than that computed from trials of afferent triggered spiking (Fig. 3b). We attribute this difference to the slight variability in depolarization generated by premotor synaptic events triggered by afferent signals that is not present when passing current directly to the motoneurons. In addition, decay in spike rate during the phase 1 burst, when triggered by afferent potentials, is more rapid than that generated by intracellular current injection (Krans and Chapple 2005).

The relationship between force production and each of the reflex parameters was examined using the above current injection protocol and the simultaneous observation of changes in junction potential amplitude and force generation. The activity of all VSMN was monitored at the motor nerve's exit from the nerve cord to ensure that no spontaneous events contributed to force production. Only one VSMN could be intracellularly penetrated per preparation so we chose to eliminate spontaneous discharge from the other VSMN by bathing the central nervous system in a high Ca^{++} high Mg^{++} saline (HCM). The action of this saline on VSMN spike rate, membrane resistance, and premotor activity was discussed in a previous report (Krans and Chapple 2005). Briefly, membrane resistance was unchanged, and spike rate and spontaneous psp rate observed at VSMN were reversibly reduced. Data from experiments using intracellular tri-phasic activation are presented in Figs. 4 and 5.

Force production in tri-phasic versus mono-phasic activation of motoneurons

An initial question was whether the VSMN spike frequency–force relationship generated by tri-phasic discharge was different from that a simpler mono-phasic depolarization (single-square pulse of depolarizing current). In the medial and central VSMN, peak force generated by the tri-phasic experimental design was always greater than force generated by a single pulse depolarization of comparable spike rate and duration (Fig. 4a). Unlike the other longitudinal muscles, the lateral VSMN innervates spiking muscles that generate far greater force. Thus the frequency–force relationship of the lateral is fundamentally different from that of the other longitudinal muscles (Krans and Chapple 2005). Data from experiments in which the lateral VSMN was intracellularly penetrated were excluded from this analysis.

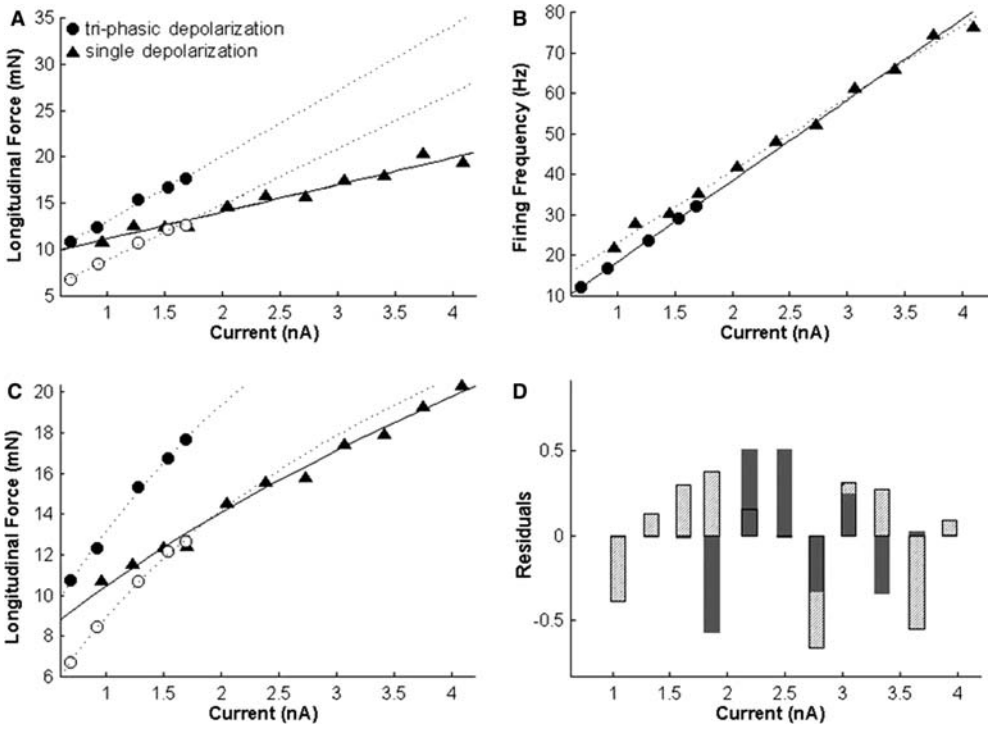

Fig. 4 Force generated by the tri-phasic reflex versus that from single phase depolarization. Longitudinal force produced by the abdominal segments increases with depolarizing current magnitude to the postural motoneurons, as depicted by these examples from the medial ventral superficial muscle motoneuron. *Circles* force generated by the tri-phasic reflex, *Triangles* force produced by single pulses of depolarizing current for a duration equivalent to that of phase 3 of the artificial reflex. The intracellular tri-phasic experimental design consists of two different current magnitudes, that of phase 1 and of phase 3; phase 2 is a return to rest. The current magnitude of phase 3 is used in these figures; the duration and number of spikes in this phase greatly out-number those of the first phase (10× duration and up to 4× number of spikes). The range of currents used in the artificial tri-phasic experiments was lesser than that in single depolarization experiments such that only portions of the current–force and current–frequency relationships overlap. *Filled circles* are total force produced by all three phases. *Open circles* represent force produced by phase 3 spiking only. **a** Using linear models to fit the current-force data, the two tri-phasic functions are significantly different from the single depolarization current-force function (*filled circle*: $y=7.02x+6.01$, *open circle*: $y=6.00x+2.81$, vs. *triangle*: $y=2.91x+8.21$; ANOCOVA, $P=0.0002$ and $P=0.0018$, respectively). **b** In contrast, linear models of the current–frequency relationships for single depolarization data and for artificial tri-phasic data are not significantly different (*filled circle*: $y=21.70x-1.67$, vs. *triangle*: $y=17.91x+5.06$ ANOCOVA, $P=0.16$). **c** Current-force data plotted in panel A were also approximated by logarithmic fits. **d** The residuals from linear and logarithmic fits are superimposed (*solid* linear, *hash* logarithmic). The norm of the residuals was not substantially different: linear norm of residuals = 1.058, and logarithmic norm of residuals = 1.037. Neither of the two models for these data provides a notably superior fit ($F=1.19$, $P=0.79$)

The slope of the current-force relationship in tri-phasic depolarization experiments was greater than that generated by a single-square pulse of depolarization to VSMN (Fig. 4a; tri-phasic data: circles; single depolarization: triangles). In tri-phasic depolarization experiments, the current magnitude of phase 3 was used for comparison to the single current injected in monophasic/single depolarization experiments (ANOCOVA, $P < 0.01$). We chose to use current rather than spike frequency as the independent variable of these

►

Fig. 5 Parameters of the intracellularly driven tri-phasic motoneuron discharge. All data in Fig. 5 are from experiments using the intracellular current injection to motoneurons (Figure 3) protocol. Excluding panel **a**, all dependent axes are normalized so that data from many preparations can be compared. Peak force is measured over the entire tri-phasic discharge, rather than within the temporal confines of a particular phase, unless specified. **a** Force, measured shortly after the end of the initial burst, increases with spike rate ($n=5$ preparations, *triangles* 400 ms after the phase 1 burst, $y=0.083x-0.056$, $r=0.95$, $P<0.01$; *circles* 100 ms after the phase 1 burst, $y=0.046x-0.16$, $r=0.87$, $P<0.01$). Standard deviation and standard error are plotted, the former bring greater than the latter. **b** Peak force generated by the entire tri-phasic protocol does not change with phase 1 frequency ($n=3$ preparations, linear model: $y=0.56x+0.32$, $r=0.39$; and logarithmic model: $y=0.39\mathrm{Ln}(x)+0.86$, $r=0.39$; $P>0.05$, both). **c** *Squares* Peak force generated by the protocol increases only slightly with phase 2 duration ($n=6$, $y=2.2\cdot10^{-4}\ x+0.86$, $r=0.58$, $P=0.041$). The change in peak force is small and variable (standard error of the mean is shown). *Triangles*: Force measured at 400 ms after the end of the phase 2, and *circles* 100 ms after phase 2. The early measures of force are fitted well by similar parabolic functions, the primary difference between them being a shift in intercept ($n=4$, *triangles*: $y=-2.5\cdot10^{-6}\ x^2+0.0013x+0.47$, $r=0.97$, $P<0.01$, and *circles* $y=-2.7\cdot10^{-6}\ x^2+0.0013x+0.37$, $r=0.94$, $P<0.01$). **d** Phase 3 mean frequency increases with phase 2 duration ($n=8$, $y=0.11\mathrm{Ln}(x)+0.34$, $r=0.77$, $P=0.008$), but the magnitude of change in mean frequency is not as notable as the range of initial phase 3 frequency, as depicted in **e** The instantaneous frequency of the first spike pair in phase 3 increases with phase 2 duration ($n=8$, $y=0.26\mathrm{Ln}(x)-0.57$, $r=0.93$, $P<0.01$). **f** Peak force generated by the protocol increases with phase 3 frequency ($n=8$, $y=0.021x+0.22$, $r=0.96$, $P<0.01$)

experiments because this was the variable that we experimentally modified (not frequency), and the current–frequency relationship was not statistically different in the two experimental designs (Fig. 4b). Mean phase 3 spike rate was always slightly less than that computed in trials of a single pulse of depolarization alone, but a comparison of the current–frequency relationships of the two revealed that they were not statistically different (Fig. 4b, ANOCOVA, $P = 0.16$). Phase 3 spike rates in afferent triggered reflex discharge—in contrast to depolarization generated discharge—rarely exceed about 30 Hz (Table 1). Whereas this limited the range of phase 3 current magnitudes investigated during tri-phasic experiments (see description of the protocol above), the range over which single pulses of depolarization was tested was much greater (Fig. 4b).

The interpretation of current–force relationships from the two experimental designs is confounded by the phase 1 spiking that is present in tri-phasic experiments but not in single pulse experiments. Among the confounding factors introduced by this inequality are: (1) the brief but high frequency spiking of phase 1 acts to facilitate ejp amplitude (Atwood and Johnston 1968; Zucker and Regehr 2002); (2) spike-frequency adaptation is elicited by phase 1 high-frequency spiking and acts to reduce spike rate during following depolarization

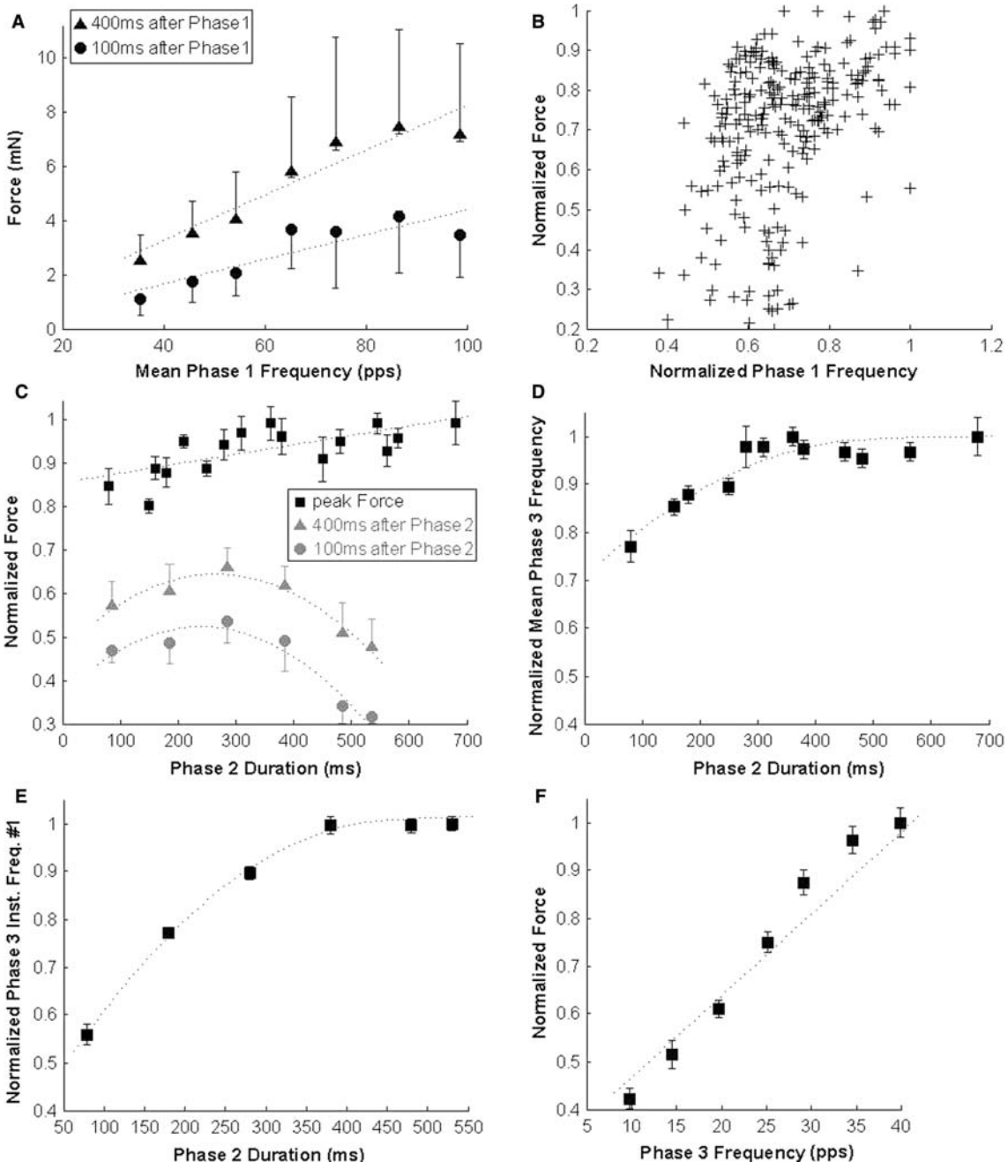

(Krans and Chapple 2005); (3) the dynamics of muscle shortening may change with motoneuron frequency and over time when activated (Chapple 1989b; Hoyle 1983; Josephson and Stokes 1994; Wakabayashi and Kuroda 1977). We were unable to directly control these factors and thus could not quantify their contributions to force production. In an effort to partially accommodate them we chose to subtract the force generated over the first 500 ms of the tri-phasic depolarization experimental design from the total (peak) force produced, deducting phase 1 generated force (Fig. 4a, c, open circles).

The major result is that in tri-phasic depolarization experiments, regardless of scaling or adjustment, the slope of the current–force relationship was steeper than in mono-phasic depolarization experiments. An analysis of covariance was performed to determine if the adjusted tri-phasic current–force relationship was statistically different from that of the mono-phasic depolarization. This was a particular concern because the models used to fit the two experimental conditions intersect, regardless of whether linear or logarithmic/exponential models were used. Both the non-adjusted and adjusted tri-phasic current–force relationships were different from mono-phasic depolarization data (ANOCOVA, $P = 0.0002$ and $P = 0.0018$, respectively). It was difficult to predict what the current-force relationship might be, so we evaluated the fit of two models that gave the smallest norm of residuals values: linear and logarithmic. Fig. 4c is a logarithmic fit of the data that is fit by a linear model in Fig. 4a. The residuals of the two functions were not significantly different (Fig. 4d, F-stat $= 1.19$, $P = 0.78$).

Relationships of tri-phasic parameters to force production

In previous work, we hypothesized that phase 1 frequency would impact force greatly (Krans and Chapple 2005). The spike rate during phase 1 begins at about 20–50 times that of tonic spontaneous output (~200–250 pps and ~5–10 pps, respectively). Depicted in Fig. 5a are phase 1 frequency-force data from five preparations in which the medial VSMN was manipulated using the intracellular tri-phasic depolarization protocol. There was a relationship between phase 1 spike rate and force when force was measured 100 and 400 ms after the termination of the initial burst ($r = 0.95$ and 0.87, respectively, $P < 0.01$ each). That relationship was lost when evaluating peak force generated by the entire tri-phasic sequence (Fig. 5a and b). Neither linear nor logarithmic models produced acceptable fits of the phase 1 frequency and peak force relationship, for which force was measured upon completion of all three phases (Fig. 5b, fit lines not shown, $P > 0.05$, both). This loss of correlation was expected; the second phase cessation of firing and the spikes of the third phase further modify force. In this and following panels of Fig. 5, frequency values and total force were normalized to the mean values for comparison across several preparations. During investigation of each parameter of reflex spiking, the other parameters were held constant at average physiological values (Table 1).

The relationship between phase 2 duration and peak tri-phasic force was variable and force increased very little as phase 2 duration increased nearly ten fold (Fig. 5c: squares, linear model, $r = 0.58$, $P = 0.04$). In contrast, the relationship between phase 2 duration and force measurements made shortly after the termination of phase 2 showed a better correlation (Fig. 5v: triangles and circles). This relationship was approximately parabolic. The parabolic change in force with phase 2 duration was anticipated; for a short period after the termination of phase 1, force continues to grow, plateaus momentarily, and then begins to decay with longer phase 2 durations (e.g. Fig. 1a). Peak force and phase 2 duration did not follow a similar model; it was better fit by a linear model (Fig. 5c: squares, $r = 0.94$ and $r = 0.97$ at 100 and 400 ms after phase 2, respectively; $P < 0.01$ each). The significance of these data being fit by a linear model is not inherent to linearity, but in the deviation from a parabolic function, as was shown when force was measured closer to the termination of phase 2. We did not expect that with long phase 2 durations, as long as 700 ms with no motoneuron spiking, force would remain constant or continue to grow.

Our recent characterization of spike frequency adaptation intrinsic to VSMN led us to hypothesize that the duration of phase 2 should be positively correlated with increasing phase 3 frequency (Krans and Chapple 2005). The repolarization of VSMN by inhibitory synaptic potentials, which is characteristic of afferent triggered phase 2, acts to alleviate the spike frequency adaptation initiated by high-frequency spiking of phase 1. Thus with increased phase 2 duration, greater spike rates may be attained from comparable underlying depolarization during phase 3. As predicted, the mean frequency of phase 3 increased with phase 2 duration (Fig. 5d, logarithmic $r = 0.77$, $P < 0.01$). However, the monotonic increase of force persisted only to a phase 2 duration of about 300 ms. The relationship between initial instantaneous frequency of phase 3 and phase 2 duration was more profound (Fig. 5e, $r = 0.93$, $P < 0.01$), persisting through phase 2 durations of about 400 ms. These results confirmed that, over a limited range, phase 3 frequency increases as a function of phase 2 duration when equivalent depolarizing current magnitudes are passed. Finally, phase 3 frequency was tightly correlated with peak force (Fig. 5f, $r = 0.96$, $P < 0.01$), which was anticipated because phase 3 is both the terminal portion of the experimental design and the longest period of depolarization, accounting for the majority of spikes during the tri-phasic routine. Peak force was always observed during or shortly after the third phase of VSMN spiking.

These results demonstrate the following paradox: phase 2 durations up to about 400 ms are well correlated with increased phase 3 frequency, and peak force can be predicted from phase 3 frequency, but phase 2 is a poor

predictor of peak force. What variable(s) reduces the efficacy of the increased phase 3 frequency—an increase that is at least partially dependent on the duration of phase 2—on final force generation?

Changes at the neuromuscular junction

Facilitation or depression at the neuromuscular junction was an initial prospect to resolve the paradoxical relationship described above. Concurrent with the increase in phase 2 duration, and the resultant phase 3 frequency, is the graded reduction of phase 3 initial ejp amplitude. We hypothesized that the two actions, increased spike rate and decreased ejp amplitude, might counteract one another, yielding a phase 2-force relationship with a slope of close to zero.

We measured ejp amplitude throughout the tri-phasic discharge to examine this hypothesis. Ejp amplitude was normalized to the maximum observed in each preparation for comparison across different individual muscle fibers and animals, which showed variable magnitudes of facilitation, a well documented phenomenon (Zucker and Regehr 2002). Ejp amplitude is facilitated to maximal values within as few as three spikes of phase 1 (Fig. 6a) but decays during phase 2 (Fig. 6b). During phase 1 bursts that consisted of more than four spikes, ejp amplitude decayed after the first few events, which we attribute at least partially to the action of synaptic depression (Josephson and Stokes 1987; Zucker and Regehr 2002). The initial ejp amplitude of phase 3 was consistently about 60% of the maximum value observed in phase 1 (Fig. 6b). Initial phase 3 ejp amplitude was never less than the completely non-facilitated amplitude observed upon a spontaneous neuromuscular event; likewise, it was always greater than the initial amplitude of phase 1 ejps (Figure 6a, b). The amplitude of the initial phase 3 ejp decreased in an approximately linear fashion as phase 2 duration increased (Fig. 6b).

Even at low frequency VSMN spiking during phase 3, ejps continue to facilitate until saturating shortly after the beginning of the phase. Figure 6c illustrates this; the first six ejp amplitudes of phase 3 were recorded and plotted as a function of time across varied phase 2 durations. The extrapolated curves are presented only to distinguish data sets, each of which is a different phase 2 duration, ranging from 100 to 550 ms (Fig. 6c). As phase 2 duration increased, so did the rate of ejp amplitude facilitation. By the sixth ejp to occur during phase 3, regardless of phase 2 duration, ejp amplitudes were similarly facilitated. These results support that the transient decrease in ejp amplitude might resolve the relationship of phase 2, phase 3, and final force production.

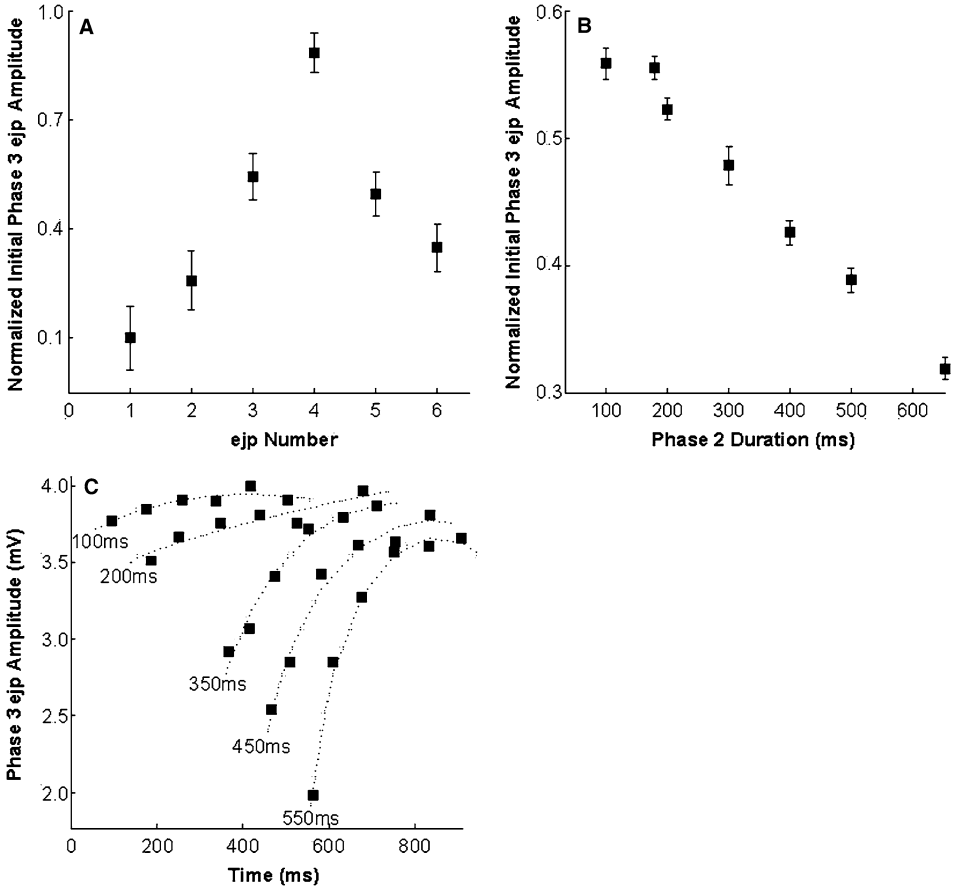

Fig. 6 Changes at the neuromuscular junction during reflex discharge **a** Ejp amplitude facilitates, then depresses in examples of phase 1 activation consisting of more than four motoneuron spikes ($n = 8$ preparations). Data are normalized to the maximum amplitude observed in a given experimental condition. **b** The amplitude of the initial phase 3 ejp decreases as phase 2 duration increases from ~100 to 700 ms ($n = 6$, $y = -0.0004x + 0.62$, $r = 0.97$, $P < 0.01$). **c** An example of phase 3 ejp facilitation in the medial ventral muscle. The phase 2 duration used to generate each of these series is labeled at its beginning. In trials with phase 2 duration greater than about 200 ms the initial phase 3 ejp amplitude decreased substantially below that measured in experiments with phase 2 duration less than 200 ms. The rate of ejp amplitude facilitation increases with phase 2 duration. *Dotted* a second-order logarithmic approximation of the data. These models are used only to distinguish the different phase 2 durations. *Error bars* standard error

Elimination of central mechanisms by axonal stimulus

We have shown that ejp amplitude decreases as phase 2 duration increases, an expected result. It follows that if the spike rate of phase 3 were fixed to a constant frequency, and phase 2 was successively increased in duration, the resultant force would decrease. As discussed, it is the attenuation of spike-frequency adaptation that we believe increases the frequency of phase 3. The time constant measured in previous experiments of the attenuation of spike frequency adaptation, via VSMN membrane repolarization, gave values around 250 ms (Krans and Chapple 2005) and thus could be counteracting the phase-2-dependent reduction in ejp amplitude (Fig. 6b).

To test this we chose to stimulate the motor root directly, preventing the centrally located and intrinsic spike-frequency adaptation from acting on phase 3 spike rate. This experimental design permitted the precise timing of spikes to the muscle such that phase 3 was made to consist of constant frequency train (Fig. 7a). Phase 1 was unchanged from a decaying rate pattern that was shown in intracellular experiments to closely model the afferent triggered pattern. At each of several phase 2 durations, phase 3 frequency was varied throughout the range established in the previous, intracellular, experiments (Fig. 5F). The expectation was that at equivalent phase 3 rates, but longer phase 2 durations, the frequency–force relationship would be decreased due to the decrease in ejp amplitude. It was essential to these experiments that the lateral VSMN was not recruited during stimulus of the motor root since it is a spiking muscle that produces much more nonlinear frequency–force relationship than the other postural muscles (Krans and Chapple 2005).

Axonal stimulus results indicate that the above postulate is not sufficient to explain the weak relationship between phase 2 and final force production. Across equal spike rates of phase 3, but increasing phase 2 durations, there was no decrease in peak force

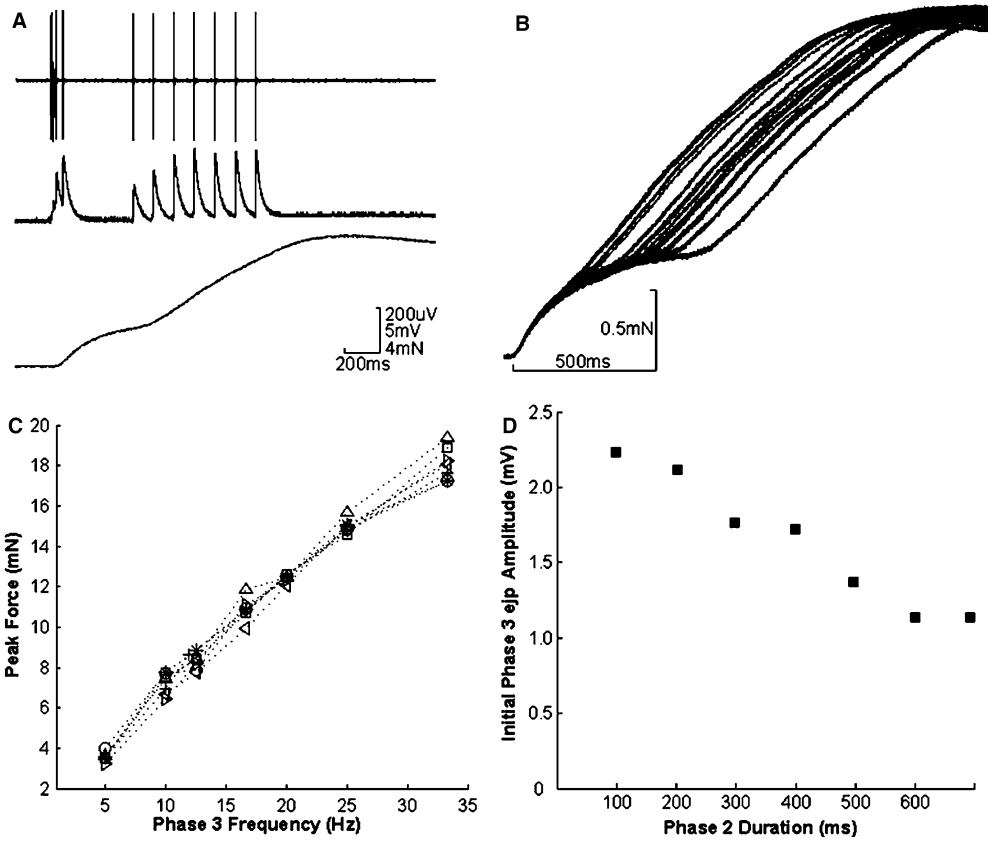

Fig. 7 Axonal stimulus model of the reflex **a** *Top* extracellular recording from the motor nerve, illustrating that only the medial motoneuron is recruited by axonal electrical stimulus. *Middle* junction potentials recorded from the medial muscle. Notice the facilitation of phase 1 and phase 3. *Bottom* force generated by the potentials depicted above. Although phase 3 frequency is about 10× less than phase 1 frequency, rate of force generation is comparable to that of phase 1. **b** There is no obvious change in peak longitudinal force or rate of force generation when phase 2 duration is varied from 90 ms to 590 ms (no other parameter of the reflex was changed). **c** Across a range of phase 2 durations there is no change in the phase 3 spike frequency—force relationship. Phase 2 durations: *cross* = 90 ms, *circle* = 190 ms, *square* = 290 ms, *upward triangle* = 390 ms, *star* = 490 ms, *rightward triangle* = 590 ms, *leftward triangle* = 690 ms. No individual frequency-force relationship is significantly different from the population ($n = 4$ preparations, ANOCOVA, population fit: $y = 0.51x + 1.93$, $P = 0.63$). **d** Similar to the case of afferent and intracellular current injection driven tri-phasic activation (see Fig. 6b), the initial phase 3 ejp amplitude recorded in axonal stimulus experiments decreases with phase 2 duration. Ejp amplitudes from one of five preparations are plotted (for all data, $n = 5$, $y = -0.0005x + 0.63$, $r = 0.91$, $P < 0.01$)

production. Phase 3 duration was held constant at 800 ms during these experiments (Fig. 7a). Figure 7b is the overlaid force traces from 15 trials in which neither phase 1 nor phase 3 spike rate was altered, but phase 2 was increased in duration. As shown, there was very little if any change in the pattern of force recruitment, and there was no change in peak force generated (t test, $P < 0.01$). Figure 7c shows the results of further analysis of these data; various phase 3 spike rates were examined across different phase 2 durations. None of the frequency-force relationships, sorted by phase 2 duration, was different from the population (Fig. 7c, ANOVA, $F = 0.03$, $P = 0.99$). An initial concern was that the amplitude of the initial ejp of phase 3 might not have appreciably decreased with phase 2 duration in these experiments. That concern was rejected upon inspection of ejp amplitude across varied phase 2 durations (Fig. 7d); ejp amplitude decreased as a function of phase 2 duration in a pattern similar to that described in intracellular tri-phasic experiments. Results from this series of experiments indicate that although ejp amplitude decreases with increased duration of phase 2, this decrease is not translated to an observable decrease in peak force production. This suggests that the phase 2 dependent increase in phase 3 spike rate is only coincidental with the decrease in ejp amplitude, and that the two opposing variables in force production do not directly counteract each other. We propose that the dynamics of muscle shortening are variable throughout the tri-phasic discharge (typically ~1 s), and that the future quantification of these variables may account for the absence of change in peak force production.

Discussion

Rapid changes in motoneuron spike rate are transformed by slow muscles during the tonic regulation of stiffness in the postural system of the *Pagurus* (Chapple 1989a, b). We have been interested in identifying the particular consequences of tri-phasic activation of the motoneurons to this behavior. From results reported here, and those in previous works (recent works of particular importance to this report are: Chapple and Krans 2004; Krans and Chapple 2005), we have adopted the following conclusions: (1) The reflex generation of force is profoundly nonlinear and the first phase may act like a switch between states. (2) The precise transformation of motor discharge to force generation remains unknown. Results suggest that further characterization of nonlinear tension development is critical to describing the transform. The general complexity of this transformation has proven difficult to quantify in several model preparations (Josephson and Stokes 1987; Morris and Hooper 1998), but remains an important and active area of research (Brezina et al. 2004, 2003a, b). (3) In the absence of an explicit transfer function, biomechanical parameters of the abdomen during tension development, and of the shell positioning system in general, must be more clearly described in order to adequately place these and similar results into a behavioral context.

The postural muscles of *Pagurus* have long time constants (e.g. Figure 1; Chapple 1989b, 1997), and these are undoubtedly a contributing factor in the lack of relationship between phase 1 frequency and duration, and tri-phasic force. Although phase 1 rarely exceeds 80–90 ms, we do not discount its importance. We hypothesize that the purpose of the rapid burst of phase 1 is to initiate facilitation at the neuromuscular junction and to initiate the increase in muscle activation in the postural muscles themselves, possibly consisting of changes in sarcomere length or phosphoralation state, as posited in other invertebrate and vertebrate models (Galler et al. 1999; Gunzel and Rathmayer 1994; Peterson et al. 2004). These changes would then substantially elevate gain in the frequency–force function for the upcoming late reflex phases of spiking. The increase in gain driven by tri-phasic firing is depicted in Fig. 4a, which shows that the slope of the current-force relationship is greater in experiments of tri-phasic activation than from single depolarizing step experiments. We have not yet examined the mechanism(s) responsible for this change quantitatively or mechanistically, nor can we address it with these data.

A pertinent example of nonlinearity in force generation comes from the literature on catch-like tension (Blaschko et al. 1931; Hoyle 1984), which remains a topic of interest in vertebrates under the guise of *residual force enhancement* (or force enhancement: (Gunzel and Rathmayer 1994; Peterson et al. 2004; Rassier and Herzog 2004)). Josephson and Stokes (1994) illustrate that in the muscles of the maxilliped of green crab, force generated by low-frequency discharge is greater when preceded by a burst of greater frequency than when that motoneuron frequency is elicited alone and they ascribe the nonlinearity to hysteresis at the muscle. This phenomenon is evident across diverse phyla [primate and mammal: (Burke et al. 1970; Goldstein and Robinson 1986); crustaceans: (Blaschko et al. 1931; Josephson and Stokes 1994; Wakabayashi and Kuroda 1977); mollusks: (Castellani and Cohen 1992; Cohen and Castellani 1988; von Uexkull 1912); cockroach: (Chesler and Fourtner 1981)]. Although the mechanism by which this tone is maintained may be triggered by pharmacological changes (octopamine: (Hoyle 1984)), the precise intramuscular mechanism remains unclear. It is proposed in many reports that an investigation of the cross-bridge dynamics is necessary for further characterization, as is it may be for *Pagurus* (Galler et al. 1999; Hoyle 1983; Rassier and Herzog 2004).

In *Pagurus*, it appears that the tri-phasic reflex operates in a way similar to the catch-like tension phenomena, excepting the maintenance of tone in the complete absence of motoneuronal activity that is reported in some species (in *Pagurus* Fig. 8; maintained tension in the absence of neuromuscular events (Hoyle and Field 1983)). This increase in tension following a

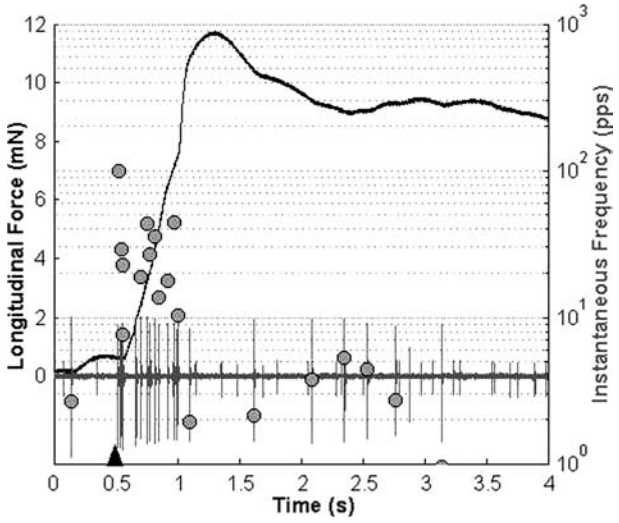

Fig. 8 Catch-like hysteresis in force production. A single example of the late phase 3 after-discharge showing extracellular activity in the motor nerve (*gray trace*), longitudinal force generated (*black*), and the instantaneous frequency of the medial VSMN (*filled circles*). In this example, an electrical stimulus of the afferent nerve was given at time = 0.5 s (*arrowhead*). Although VSMN spike rate (*circles*) returns to approximately prestimulus values after about 500 ms of reflex spiking, force remains elevated at nearly 10× the initial value for several seconds thereafter. This resembles catch-like tension, which is discussed in text

brief burst of potentials has been reported to last from several seconds to several minutes in other insects and crustacea (Hoyle and Field 1983; Wilson and Larimer 1968). Those periods are longer than what we have observed in *Pagurus*, but are similar within an order of magnitude (elevated tone for ~3.2 s, Fig. 8, re-scaled from Krans and Chapple (2005). One possibility is that reduced preparations reduce this time; recent investigations of phase 3 have been made in the isolated abdomen or individual segments. Unlike the majority of preparations in which catch-like tension has been examined, *Pagurus* is a tonic system involved in the execution of slow postural tasks. Relative to the motor demands of reaching or grasping, supporting a gastropod shell is a continuous affair. However, one functional explanation for the peripheral control of gain in the frequency–force relationship is the ability to shift between states, such as mobile and immobile, without change in premotor integration. Recent observations of behaving *Pagurus* support this hypothesis (unpublished videographic studies performed by E.W. Kelly, J.L. Krans and W.D. Chapple). The shape and size of the abdomen, when examined in these behavioral experiments, change dramatically upon animal-induced movement, but otherwise remain fairly consistent in the presence of light mechanical disruption of the shell while at rest. Changing gain of the frequency–force relationship at a peripheral location would reduce the necessity for changes made in centrally located integration elements such that comparable premotor signals yield grossly dissimilar force production.

In the final series of experiments reported here, we show that a decrease in ejp amplitude, alone, does not reduce force production in the third phase of reflex discharge (Fig. 7). In addition to ejp amplitude, we examined the temporal summation of these potentials. The increase in membrane potential from which each new ejp during phase 3 began was nominal in all experiments and not significantly related to either phase 3 rate or force generated. In addition, integration of VSM membrane potential from the start time to the end time of phase 3 gave no correlation with either phase 3 rate or force generation. These results are not surprising; in any given experiment, no two penetrations of VSM gave equivalent ejp amplitudes (possibly a simple product of length constants) or facilitation rates. Variation in neuromuscular junction size and efficacy from junction to junction is a well-documented phenomenon (Millar et al. 2002; Zucker and Regehr 2002). The global change in membrane potential of the muscle is thus difficult to assess from individual and local intracellular penetrations.

The way that tonic motor systems compensate for peripheral changes in the midst of intrinsic (motoneuron) and extrinsic changes (hysteresis) to the system itself remains poorly understood. Future investigation of the mechanisms by which gain in the frequency–force relationship changes during reflex activation, and the ways this phenomenon is modulated, may provide useful comparative insight.

Acknowledgements We thank Dr. Andrew Moiseff for critical commentary and Elizabeth W. Kelly for her assistance in preparing the manuscript. Ms. Kelly also contributed via her behavioral observations of *Pagurus* and the establishment of methods necessary in those endeavors. We thank Joseph Healy, who supplied us with *Pagurus pollicarus*.

References

Atwood HL (1967) Crustacean neuromuscular mechanisms. Am Zool 7:527–552

Atwood HL, Johnston H (1968) Neuromuscular synapses of a crab motor axon. J Exp Zool 167:457– 470

Beloozerova IN, Zelenin PV, Popova LB, Orlovsky GN, Grillner S, Deliagina TG (2003) Postural control in the rabbit maintaining balance on the tilting platform. J Neurophysiol 90:3783–3793

Blaschko H, Cattell M, Kahn JL (1931) On the nature of the two types of response in the neuromuscular system of the crustacean claw. J Physiol 73:25–35

Brezina V, Orekhova IV, Weiss KR (2003a) Neuromuscular modulation in *Aplysia*. I. Dynamic model. J Neurophysiol 90:592–2612

Brezina V, Orekhova IV, Weiss KR (2003b) Neuromuscular modulation in *Aplysia*. II. Modulation of the neuromuscular transform in behavior. J Neurophysiol 90:2613–2628

Brezina V, Horn CC, Weiss KR (2004) Modeling neuromuscular modulation in *Aplysia* III. Interaction of central motor commands and peripheral modulatory state for optimal behavior. J Neurophysiol, Articles in Print jn.00475.2004

Burke RE, Rudomin P, Zajac FE III (1970) Catch property in single mammalian motor units. Science 168:122–124

Castellani L, Cohen C (1992) A calcineurin-like phosphatase is required for catch contraction. FEBS Lett 309:321–326

Chapple WD (1973a) Changes in abdominal motoneuron frequency correlated with changes of shell position in the hermit crab, *Pagurus pollicarus*. J Comp Physiol 87:49–64
Chapple WD (1973b) Role of the abdomen in the regulation of shell position in the hermit crab *Pagurus pollicarus*. J Comp Physiol 82:317–332
Chapple WD (1989a) Mechanics of stretch in activated crustacean slow muscle. I. Factors affecting peak force. J Neurophysiol 62:997–1005
Chapple WD (1989b) Mechanics of stretch in activated crustacean slow muscle. Ii. Dynamic changes in force in response to stretch. J Neurophysiol 62:1006–1017
Chapple WD (1997) Regulation of muscle stiffness during periodic length changes in the isolated abdomen of the hermit crab. J Neurophysiol 78:1491–1503
Chapple WD, Krans JL (2004) Cuticular receptor activation of postural motoneurons in the abdomen of the hermit crab, *Pagurus pollicarus*. J Comp Physiol A 190:365–377
Chesler M, Fourtner CR (1981) Mechanical properties of a slow muscle in the cockroach. J Neurobiol 12:391–402
Cohen C, Castellani L (1988) New perspectives on catch. Comp Biochem Physiol C 91:31–33
Fung J, Macpherson JM (1999) Attributes of quiet stance in the chronic spinal cat. J Neurophysiol 82:3056–3065
Galler S, Kogler H, Ivemeyer M, Ruegg JC (1999) Force responses of skinned molluscan catch muscle following photoliberation of ATP. Pflugers Arch 438:525–530
Goldstein HP, Robinson DA (1986) Hysteresis and slow drift in abducens unit activity. J Neurophysiol 55:1044–1056
Gunzel D, Rathmayer W (1994) Non-uniformity of sarcomere lengths can explain the 'catch-like' effect of arthropod muscle. J Muscle Res Cell Motil 15:535–546
Harris-Warrick R, Kravitz E (1984) Cellular mechanisms for modulation of posture by octopamine and serotonin in the lobster. J Neurosci 4:1976–1993
Horak F, MacPherson J (1996) *Postural orientation and equilibrium*. In: Rowell L, Shepherd J (eds) Handbook of physiology. Oxford Press, New York, pp 255–292
Hoyle G (1983) Forms of modulatable tension in skeletal muscles. Comp Biochem Physiol A 76:203–210
Hoyle G (1984) Neuromuscular transmission in a primitive insect: modulation by octopamine, and catch-like tension. Comp Biochem Physiol C 77:219–232
Hoyle G, Field LH (1983) Defense posture and leg-position learning in a primitive insect utilize catchlike tension. J Neurobiol 14:285–298
Josephson RK, Stokes DR (1987) The contractile properties of a crab repiratory muscle. J Exp Biol 131:265–287
Josephson RK, Stokes DR (1994) Contractile properties of a high-frequency muscle from a crustacean—mechanical power output. J Exp Biol 187:295–303
Kitabayashi N, Kusunoki Y, Gunji YP (2002) Active behavior and 1/f noise in shell-changing behavior of the hermit crabs. Riv Biol 95:327–336
Krans JL, Chapple WD (2005) The action of spike frequency adaptation in the postural motoneurons of hermit crab abdomen during the first phase of reflex activation. J Comp Physiol A, DOI: 10.1007/s00359-004-0581–9
Ma P, Beltz B, Kravitz E (1992) Serotonin-containing neurons in lobsters: their role as gain-setters in postural control mechanisms. J Neurophysiol 68:36–54
Magarinos-Ascone C, Nunez A, Delgado-Garcia JM (1999) Different discharge properties of rat facial nucleus motoneurons. Neuroscience 94:879–886
Millar AG, Bradacs H, Charlton MP, Atwood HL (2002) Inverse relationship between release probability and readily releasable vesicles in depressing and facilitating synapses. J Neurosci 22:9661–9667
Morris LG, Hooper SL (1998) Muscle response to changing neuronal input in the lobster (*Panulirus interruptus*) stomatogastric system: slow muscle properties can transform rhythmic input into tonic output. J Neurosci 18:3433–3442
Noah JA, Quimby L, Frazier SF, Zill SN (2004) Sensing the effect of body load in legs: responses of tibial campaniform sensilla to forces applied to the thorax in freely standing cockroaches. J Comp Physiol A 190:201–215
Peterson DR, Rassier DE, Herzog W (2004) Force enhancement in single skeletal muscle fibres on the ascending limb of the force–length relationship. J Exp Biol 207:2787–2791
Rassier DE, Herzog W (2004) Active force inhibition and stretch-induced force enhancement in frog muscle treated with bdm. J Appl Physiol 97:1395–1400
Ridgel AL, Frazier SF, DiCaprio RA, Zill SN (2000) Encoding of forces by cockroach tibial campaniform sensilla: Implications in dynamic control of posture and locomotion. J Comp Physiol A 186:359–374
Turra A, Denadai MR (2002) Substrate use and selection in sympatric intertidal hermit crab species. Braz J Biol 62:107–112
von Uexkull J (1912) Studien über den tonus. Vi. Die pilgermuschel. Z Biol 58:305–332
Wakabayashi T, Kuroda T (1977) Responses of crayfish muscle preparations to nerve stimulation with various patterns of impulse sequence. Effects of intermittent, intercalated and adaptational types of impulse sequence. Tohoku J Exp Med 121:207–218
Wilson DM, Larimer JL (1968) The catch property of ordinary muscle. Proc Natl Acad Sci USA 61:909–916
Zill SN (1987) Selective mechanical stimulation of an identified proprioceptor in freely moving locusts: role of resistance reflexes in active posture. Brain Res 417:195–198
Zucker RS, Regehr WG (2002) Short-term synaptic plasticity. Annu Rev Physiol 64:355–405